DOI: 10.1002/ejic.201000836

Synthesis and Characterisation of Novel (Guanidine)manganese Complexes and Their Application in the Epoxidation of 1-Octene

Ramona Wortmann,[a] Ulrich Flörke,[a] Biprajit Sarkar,[b] Venkatesan Umamaheshwari,[c] Georg Gescheidt,[c] Sonja Herres-Pawlis,*[d] and Gerald Henkel*[a]

Keywords: Epoxidation / Manganese / Guanidine ligands / Alkenes

The synthesis of manganese complexes of the guanidine–pyridine hybrid ligands DMEGqu (**L1**) and TMGqu (**L2**) is reported. The complexes $[Mn_2(\mu\text{-}Cl)_2Cl_2(DMEGqu)_2]$ (**C1**), $[Mn_2(TMGqu)_2(\mu\text{-}Cl)_2Cl_2]$ (**C2**), $[Mn_3(DMEGqu)_2(\mu\text{-}CH_3COO)_6]$ (**C3**), $[Mn_3(TMGqu)_2(\mu\text{-}CH_3COO)_6]$ (**C4**) and $[Mn_2(DMEGqu)_2(\mu\text{-}CF_3SO_3)_2(CF_3SO_3)_2(H_2O)_2]$ (**C5**) have been structurally characterised. For **C1** and **C2** dinuclear chlorido-bridged motifs have been found and trinuclear acetato-bridged motifs for **C3** and **C4** which represent the first trinuclear (guanidine)manganese compounds reported so far. The dinuclear triflato complex **C5** exhibits a unique $Mn(\mu\text{-}CF_3SO_3)_2(CF_3SO_3)_2$ unit. EPR measurements of **C1** and **C2** indicate that in solution the dinuclear complexes decompose to mononuclear species. Contrastingly, the EPR spectra of **C3** and **C4** show that these acetato complexes remain polynuclear in CH_3CN. The chlorido and acetato complexes convince by their high stability towards air. All complexes reported herein were screened regarding their activity in the epoxidation of 1-octene with peracetic acid. It could be proven that these compounds are able to act as catalysts in this reaction already under mild conditions. Kinetic measurements exhibit that the epoxidation reaction proceeds on a time scale interesting for industrial application.

Introduction

Metal catalysed epoxidation is an important and widely studied reaction in organic synthesis, because the resulting epoxides are useful intermediates for the chemical industry. In spite of numerous efforts in this field, there is still an increasing motivation to develop efficient, selective, inexpensive and non-toxic catalysts which already work at mild conditions. Furthermore, it is important with regard to green chemistry that they are easy to prepare, stable and work for a wide scope of alkenes. Manganese complexes are notably interesting, because they combine catalytic activity with non-toxicity. Consequently, a series of manganese complexes with different ligand systems has already been tested, for example salens, porphyrins and other N donors and also simple Mn sources like $Mn(ClO)_4$.[1,2]

[a] Department Chemie, Universität Paderborn,
Warburger Straße 100, 33098 Paderborn, Germany
Fax: +49-5251-603423
E-mail: biohenkel@uni-paderborn.de
[b] Institut für Anorganische Chemie, Universität Stuttgart,
Pfaffenwaldring 55, 70569 Stuttgart, Germany
[c] Institut für Physikalische und Theoretische Chemie, Technische Universität Graz,
Stremayrgasse 9, 8010 Graz, Austria
[d] Fakultät Chemie, Anorganische Chemie, Technische Universität Dortmund,
44221 Dortmund, Germany
Fax: +49-231-7555048
E-mail: sonja.herres-pawlis@tu-dortmund.de

Besides oxygen, hydrogen peroxide is the oxidant of first choice because of its high atom economy, low toxicity, low cost and it produces only water as by-product. But the catalase-like activity of many transition metals often prevents the use of hydrogen peroxide. Peracetic acid represents an attractive alternative which only generates acetic acid as by-product. Therefore current research interests focus on transition metal catalysts which make efficient use of peracetic acid.[3–7] For example Stack et al. investigated a series of manganese and iron systems as epoxidation catalysts with peracetic acid.[3] Chang et al. made use of trinuclear manganese complexes and Watkinson et al. tested catalytic systems based on a bipyridyl core in combination with peracetic acid.[4,5] Their results reveal that a wide scope of olefins can be epoxidised with peracetic acid, also terminal and electron-deficient substrates.

For many catalytically active epoxidation systems high-valent intermediates are proposed.[1,8] Encouraged by the promising results with guanidine ligands for the stabilisation of high-valent species,[9,10] we directed our research towards the synthesis of (guanidine)manganese complexes.[11] We envisioned that this ligand family is highly capable to stabilise manganese complexes which act as efficient epoxidation catalysts. Structural studies on (guanidine)manganese complexes have already been performed for few examples with bis- and tris(guanidines).[10–12] For our present study we utilise guanidine–pyridine hybrid ligands, which combine the excellent donor properties of guanidines

with additional coordination space for the pre-coordination of substrates. Moreover, guanidine ligands exhibit a modular and facile synthesis protocol, which offers different spacer and guanidine groups and thus admits a flexible ligand design.[13]

In order to provide a suited coordination environment for manganese, we combined a quinolyl unit with guanidine functionalities which results in the guanidine–pyridine hybrid ligands *N*-(1,3-dimethylimidazolidin-2-ylidene)quinolin-8-amine (DMEGqu, **L1**) and 1,1,3,3-tetramethyl-2-(quinolin-8-yl)guanidine (TMGqu, **L2**) (Scheme 1).[14]

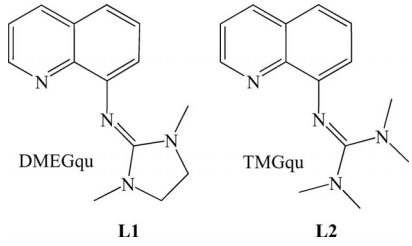

Scheme 1. Guanidine–pyridine hybrid ligands DMEGqu and TMGqu.[14]

Herein we report the synthesis and characterisation of the first manganese complexes including the guanidine–pyridine hybrid ligands DMEGqu and TMGqu. The structural characterisation has been performed for the (chlorido)-, (acetato)- and (triflato)manganese complexes **C1**–**C5** (Scheme 2). These stable complexes were screened towards their catalytic activities in the epoxidation of 1-octene with peracetic acid.

Results and Discussion

Synthesis and Characterisation of Manganese Complexes

We already described the synthesis of the guanidine–pyridine hybrid ligands DMEGqu and TMGqu by condensation of *N*,*N*′-dimethylethylenechloroformamidinium chloride (DMEG) and *N*,*N*,*N*′,*N*′-tetramethylchloroformamidinium chloride (TMG) with 8-aminoquinoline in high yields of up to 98%.[14] Their reaction with $MnCl_2 \cdot 4H_2O$, $Mn(CH_3COO)_2 \cdot 4H_2O$ and $Mn(CF_3SO_3)_2 \cdot H_2O$ in CH_3CN resulted in the formation of the di- and trinuclear manganese complexes $[Mn_2(DMEGqu)_2(\mu\text{-}Cl)_2Cl_2]$ (**C1**), $[Mn_2(TMGqu)_2(\mu\text{-}Cl)_2Cl_2]$ (**C2**), $[Mn_3(DMEGqu)_2(\mu\text{-}CH_3COO)_6]$ (**C3**), $[Mn_3(TMGqu)_2(\mu\text{-}CH_3COO)_6]$ (**C4**) and $[Mn_2(DMEGqu)_2(\mu\text{-}CF_3SO_3)_2(CF_3SO_3)_2(H_2O)_2]$ (**C5**) (Scheme 2).

The molecular structures of the compounds **C1**–**C5** (Figures 1–5) were determined by single crystal structure analysis. The corresponding TMGqu complex with $Mn(CF_3SO_3)_2$ could not be crystallised in sufficient quality yet. Selected bond lengths and angles of the characterised complexes are collected in Table 1. Further crystallographic information is summarized in Table 4.

Crystal Structures

[Mn₂L₂(μ-Cl)₂Cl₂]

In the dinuclear complexes $[Mn_2(DMEGqu)_2(\mu\text{-}Cl)_2Cl_2]$ (**C1**) and $[Mn_2(TMGqu)_2(\mu\text{-}Cl)_2Cl_2]$ (**C2**) (see Figures 1 and 2, Table 1) the Mn^{II} atoms are five-coordinate and bridged by two chloride ligands. Two further coordination sites are occupied by the N donor atoms of the hybrid guanidine ligand forming a five-membered chelate ring. The remaining coordination site is occupied by a terminal chlorido ligand. The coordination environment of the Mn atoms can be described as distorted trigonal bipyramid which is indicated by the structural parameter τ (**C1**: τ = 0.618; **C2**: τ = 0.751), introduced by Reedijk et al. (τ = 0 ideal square-pyramidal

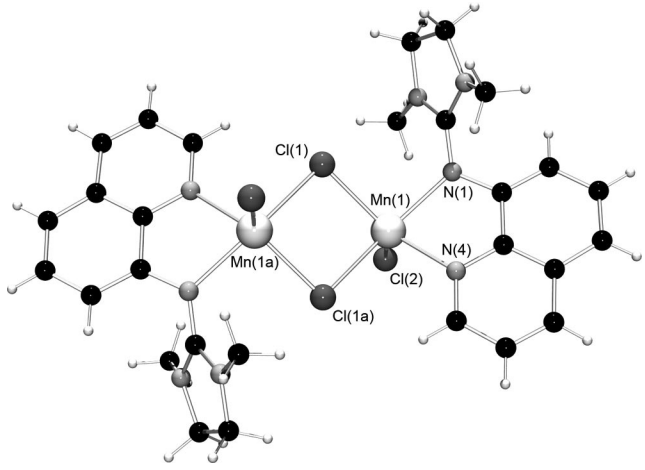

Figure 1. Molecular structure of $[Mn_2(DMEGqu)_2(\mu\text{-}Cl)_2Cl_2]$ (**C1**) as determined at 243 K (1 – *x*, –*y*, *z* + 1).

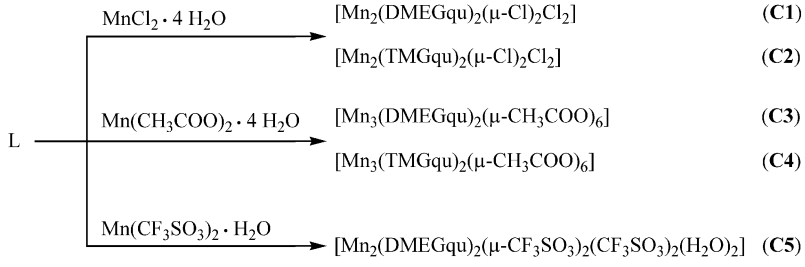

Scheme 2. Synthesis of the guanidine–pyridine hybrid ligand stabilised manganese complexes **C1**–**C5** (L = DMEGqu or TMGqu).

geometry; τ = 1 perfect trigonal-bipyramidal geometry).[15] The planar Mn_2Cl_4 unit forms a rhomb with a crystallographic inversion centre. The rhomb is determined by the Mn–Cl–Mn angle of 96.30(2) for **C1** and 93.76(2)° for **C2** and by the different values of the Mn–Cl bonds to the bridging chlorido ions [2.455(1) and 2.574(1) Å in **C1**, 2.481(1) and 2.499(1) Å in **C2**]. The bonds are in the range of other complexes containing a $Mn_2(\mu\text{-}Cl)_2Cl_2$ core.[6,16–19] In the literature a series of dinuclear Mn^{II} complexes with this chlorido-bridging motif is described, but the majority of these complexes are six-coordinate[16] and also polymeric structures are reported.[17,18] There are only few further examples of five-coordinate Mn complexes with a $Mn_2(\mu\text{-}Cl)_2Cl_2$ core.[6,19] In agreement with the reported five coordinated complexes, the terminal Mn–Cl bonds are with 2.366(1) (**C1**) and 2.372(1) Å (**C2**) shorter than the bridging ones. The Mn···Mn distance is in **C2** with 3.635(1) Å shorter than in **C1** [3.747(1) Å] and also shorter than in other complexes. This is accompanied by a larger Cl–Mn–Cl angle for **C2** [86.24(2)°] in comparison to **C1** [83.70(2)°] and the other five-coordinate complexes.[6,19] With regard to the Mn···Mn vector, the $Mn_2(\mu\text{-}Cl)_2Cl_2$ core in **C2** is more contracted than in **C1**. The bite angles defined by the quinoline ligands are with 75.34(6) and 75.73(5)° nearly identical in both complexes.

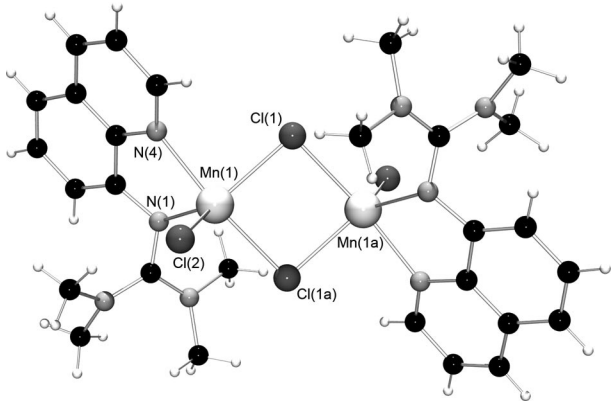

Figure 2. Molecular structure of $[Mn_2(TMGqu)_2(\mu\text{-}Cl)_2Cl_2]$ (**C2**) as determined at 120 K (1 – x + 1, –y + 2, –z).

Table 1. Selected bond lengths [Å] and angles [°] for the complexes **C1**–**C5**.

C1			
Mn(1)–N(1)	2.214(2)	Mn(1)···Mn(1a)	3.747(1)
Mn(1)–N(4)	2.215(2)	N(1)–Mn(1)–N(4)	75.34(6)
Mn(1)–Cl(1)	2.455(1)	Cl(1)–Mn(1)–Cl(1a)	83.70(2)
Mn(1)–Cl(1a)	2.574(1)	Mn(1)–Cl(1)–Mn(1a)	96.30(2)
Mn(1)–Cl(2)	2.366(1)		
C2			
Mn(1)–N(1)	2.189(1)	Mn(1)···Mn(1a)	3.635(1)
Mn(1)–N(4)	2.220(1)	N(1)–Mn(1)–N(4)	75.73(5)
Mn(1)–Cl(1)	2.481(1)	Cl(1)–Mn(1)–Cl(1a)	86.24(2)
Mn(1)–Cl(1a)	2.499(1)	Mn(1)–Cl(1)–Mn(1a)	93.76(2)
Mn(1)–Cl(2)	2.372(1)		
C3			
Mn(1)–N(1)	2.289(1)	Mn(1)···O(6)	2.691(2)
Mn(1)–N(4)	2.188(1)	Mn(1)···Mn(2)	3.545(1)
Mn(1)–O(1)	2.115(1)	N(1)–Mn(1)–N(4)	74.70(5)
Mn(1)–O(5)	2.123(1)	Mn(1)–O(5)–Mn(2)	110.45(5)
C4			
Mn(1)–N(1)	2.283(2)	Mn(1)···O(5)	2.411(2)
Mn(1)–N(4)	2.203(2)	Mn(1)···Mn(2)	3.576(1)
Mn(1)–O(1)	2.107(2)	N(1)–Mn(1)–N(4)	74.59(9)
Mn(1)–O(6)	2.183(2)	Mn(1)–O(6)–Mn(2)	109.38(8)
C5			
Mn(1)–N(1)	2.172(2)	Mn(1)–O(1)	2.200(1)
Mn(1)–N(4)	2.197(2)	Mn(1)···Mn(1a)	5.661(1)
Mn(1)–O(4)	2.167(1)	N(1)–Mn(1)–N(4)	77.24(6)
Mn(1)–O(6a)	2.380(1)	O(4)–Mn(1)–O(6a)	83.85(5)

[$Mn_3L_2(\mu\text{-}CH_3COO)_6$]

The structures of the acetato complexes $[Mn_3(DMEGqu)_2(\mu\text{-}CH_3COO)_6]$ (**C3**) and $[Mn_3(TMGqu)_2(\mu\text{-}CH_3COO)_6]$ (**C4**) are depicted in Figure 3 and Figure 4. In the trinuclear complexes with linear Mn arrangement each pair of manganese atoms is bridged by three μ-acetato ligands, two of them coordinate in a bidentate fashion and one in a monodentate mode. The central manganese atom is coordinated octahedrally by six oxygen atoms of the acetato ligands and is located on a crystallographic inversion centre. The terminal manganese atoms are five-fold coordinated by three oxygen atoms and two N donor atoms of the hybrid guanidine ligands. Additionally, the free oxygen atom of the monodentate acetate interacts weakly with the terminal Mn^{II} atoms. Therefore it can be described as [5 + 1] coordination. The coordination geometry is nearly a square pyramid (**C3**: τ = 0.24; **C4**: τ = 0.19). Taking the 6th weakly bound ligand into account, the coordination sphere resembles a distorted octahedron. The distance to the weakly bound oxygen is in **C4** with 2.411(2) Å significantly shorter than in **C3** with 2.691(2) Å. On the contrary, the bond of this manganese atom to the monodentate bridging oxygen atom is in **C3** [2.123(1) Å] shorter than in **C4** [2.183(2) Å]. This is in accordance with the "carboxylate shift" described by Lippard et al.[20] The Mn(1)–O(5) bond in **C3** is one of the shortest and the Mn(1)–O(6) bond belongs to the largest for this binding motif.[4,18,21,22] Remarkable is that in $[Mn_3(pybim)_2(CH_3COO)_6]$ the Mn–O bond to the bridging

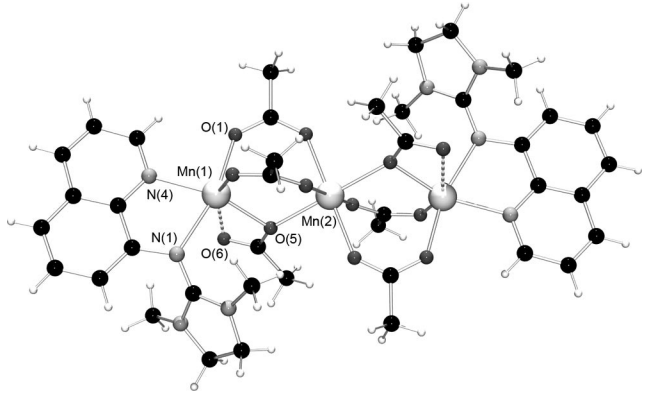

Figure 3. Molecular structure of $[Mn_3(DMEGqu)_2(\mu\text{-}CH_3COO)_6]$ (**C3**) as determined at 120 K (1 – x + 1, –y + 2, –z).

oxygen atom is also very short (2.132 Å), but the Mn···O distance of the free oxygen atom is notably larger (2.823 Å) than in **C3**.[22] The Mn···Mn distances of **C3** and **C4** are with 3.545(1) (**C3**) and 3.576(1) Å (**C4**) in the range of analogous complexes.[4,18,21,22] The described $[Mn_3(CH_3COO)_6]$ unit is also part of the polymeric $Mn(CH_3COO)_2{\cdot}4H_2O$ structure, but here the second oxygen of the monodentate bridging acetato ligand coordinates to a manganese atom of a further $[Mn_3(CH_3COO)_6]$ unit.[23]

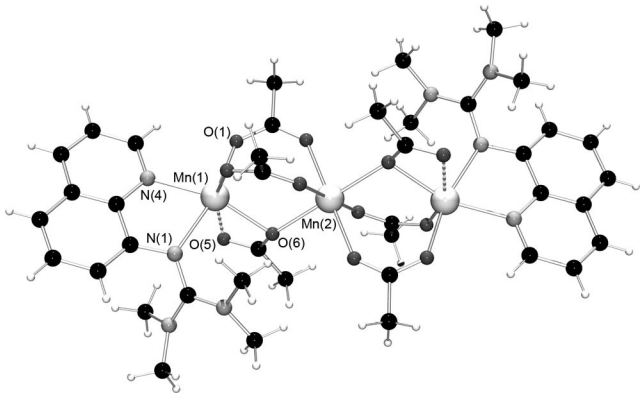

Figure 4. Molecular structure of $[Mn_3(TMGqu)_2(\mu\text{-}CH_3COO)_6]$ (**C4**) as determined at 120 K (1 – *x* + 2, –*y*, –*z*).

[Mn₂L₂(μ-CF₃SO₃)₂(CF₃SO₃)₂(H₂O)₂]

The structure of the dinuclear inversion symmetric complex $[Mn_2(DMEGqu)_2(\mu\text{-}CF_3SO_3)_2(CF_3SO_3)_2(H_2O)_2]$ (**C5**) is shown in Figure 5. The manganese atoms have an octahe-

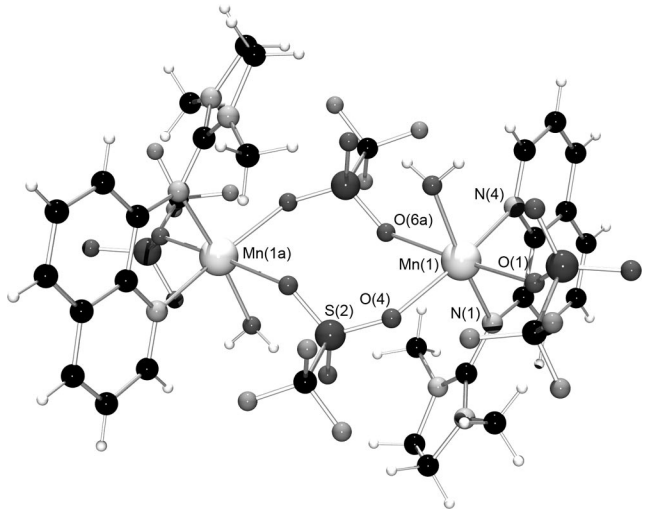

Figure 5. Molecular structure of $[Mn_2(DMEGqu)_2(\mu\text{-}CF_3SO_3)_2(CF_3SO_3)_2(H_2O)_2]$ (**C5**) as determined at 120 K (1 – *x* + 1, –*y* + 1, –*z* + 1).

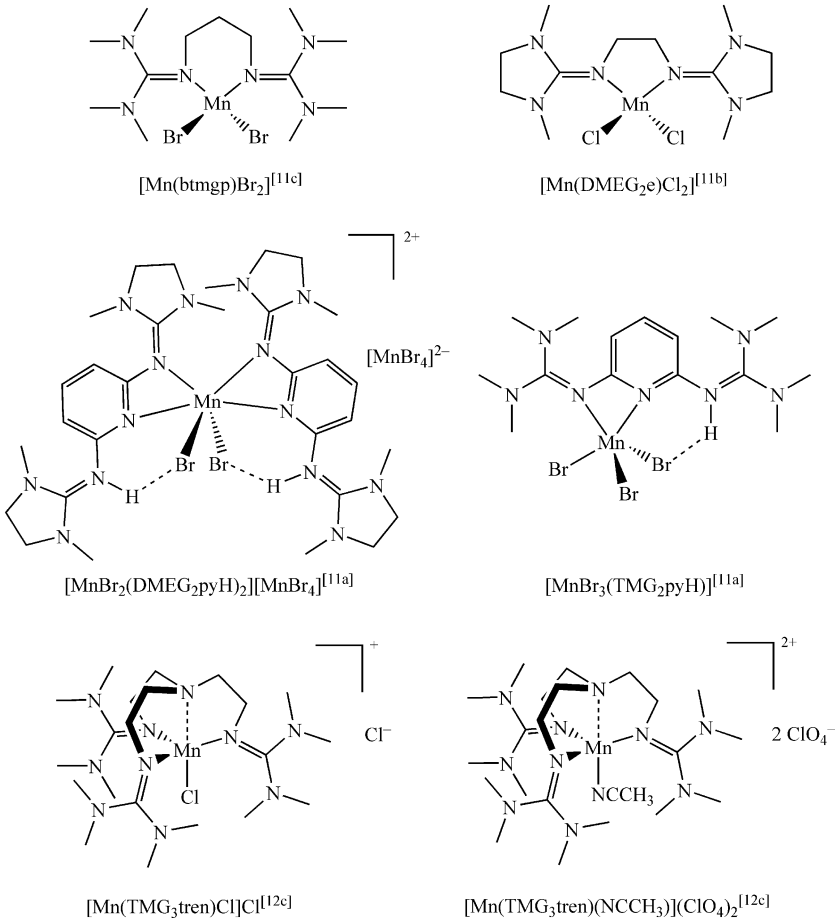

Scheme 3. Discussed (guanidine)manganese complexes.

Table 2. Selected bond lengths [Å] and ρ values of different (guanidine)manganese complexes.

	Mn–N_{gua}	C=N_{imine}	C–N_{amine1}	C–N_{amine2}	ρ	cn	Ref.
$[Mn_2(DMEGqu)_2(\mu\text{-}Cl)_2Cl_2]$ (**C1**)	2.214(2)	1.333(2)	1.329(3)	1.353(2)	0.994	5	
$[Mn_2(TMGqu)_2(\mu\text{-}Cl)_2Cl_2]$ (**C2**)	2.189(1)	1.352(2)	1.354(2)	1.339(2)	1.004	5	
$[Mn_3(DMEGqu)_2(\mu\text{-}CH_3COO)_6]$ (**C3**)	2.289(1)	1.324(2)	1.354(2)	1.339(2)	0.983	5 + 1	
$[Mn_3(TMGqu)_2(\mu\text{-}CH_3COO)_6]$ (**C4**)	2.283(2)	1.332(4)	1.348(4)	1.360(4)	0.984	5 + 1	
$[Mn_2(DMEGqu)_2(\mu\text{-}CF_3SO_3)_2(CF_3SO_3)_2(H_2O)_2]$ (**C5**)	2.172(2)	1.338(2)	1.339(3)	1.345(3)	0.997	6	
[Mn(btmgp)Br_2]	2.098(1)	1.313(2)	1.361(2)	1.356(2)	0.967	4	[11c]
	2.103(1)	1.312(2)	1.360(2)	1.359(2)	0.966		
[Mn($DMEG_2$e)Cl_2]	2.139(2)	1.308(3)	1.367(3)	1.374(3)	0.954	4	[11b]
	2.139(2)						
$[MnBr_2(DMEG_2pyH)_2][MnBr_4]$	2.263(3)	1.343(5)	1.338(5)	1.340(5)	1.003	6	[11a]
	2.367(3)						
$[MnBr_3(TMG_2pyH)]$	2.264(5)	1.328(8)	1.324(8)	1.354(8)	1.003	5	[11a]
[Mn(TMG_3tren)Cl]Cl	2.182(2)	1.319	1.355	1.369	0.968	5	[12c]
	2.177(1)	1.318	1.365	1.368	0.956		
	2.191(2)	1.309	1.365	1.373	0.964		
[Mn(TMG_3tren)(NCMe)]$(ClO_4)_2$	2.127(3)	1.317	1.359	1.365	0.967	5	[12c]
	2.148(3)	1.311	1.359	1.362	0.964		
	2.131(3)	1.305	1.358	1.362	0.960		

drally distorted coordination environment. Each manganese is bound to two bridging triflato ligands and one terminal triflato ligand, the other coordination sites are occupied by the two N donor atoms of the hybrid guanidine ligand and one water. Due to the bulky triflato bridge the Mn···Mn distance is very large [5.661(1) Å]. The distance of the Mn atoms to the N_{gua} atoms is with 2.172(2) Å shorter than the binding to the N_{py} atoms [2.197(2) Å] and it is the shortest Mn–N_{gua} bond within the complexes reported herein [2.189(1) in **C2**, 2.289(1) Å in **C3**]. To the best of our knowledge this is the first manganese complex with such a bridging motif.

Until now, only few examples of (guanidine)manganese complexes are reported (Scheme 3). Therein the guanidines enable a multitude of coordination modes of manganese and the complexes exhibit a variety of coordination numbers and spacer motifs.[10–12] Known (guanidine)manganese complexes are mainly mononuclear and some are dinuclear. **C3** and **C4** are the first trinuclear (guanidine)manganese complexes. In Table 2 the structural details of guanidine binding in (guanidine)manganese complexes are summarized. Remarkably, the length of the C=N bonds ranges from 1.313(2) in [Mn(btmgp)Br_2][11] to 1.352(2) Å in **C2**. For the evaluation of the elongation of the C=N double bond and the shortening of the C–NR_2 bonds within the guanidine unit, the ρ value was introduced by Sundermeyer al at.[24] It is calculated by the formula $\rho = 2a/(b + c)$ wherein a is the C=N distance and b and c are the C–NR_2 distances. In the case of a C_3-symmetrical CN_3 unit ρ is equal to 1. As is evident in Table 2, in the complexes **C1**, **C2**, **C5**, $[MnBr_2(DMEG_2pyH)_2][MnBr_4]$ and $[MnBr_3(TMG_2pyH)]$ ρ amounts approximately 1 indicating a total delocalisation.[11] Normally, a total delocalisation goes along with a real nivellation of the bond lengths {e.g. **C5** and $[MnBr_2(DMEG_2pyH)_2]$ $[MnBr_4]$}.[11] In case of **C2** the former C=N bond is more localised between the C_{gua} atom and one of the N_{amine} atoms whereas in **C1** and $[MnBr_3(TMG_2pyH)]$ one C–N_{amine} bond is significantly longer than the other two C–N bonds. Generally, the delocalisation in complexes containing aliphatic guanidines (such as btmgp, $DMEG_2$e and TMG_3tren) is less distinct than in complexes with aromatic guanidines (such as DMEGqu and $DMEG_2$py).[11,12]

EPR Measurements

For further characterisation of the complexes and to clarify if the complexes are still polynuclear in solution,

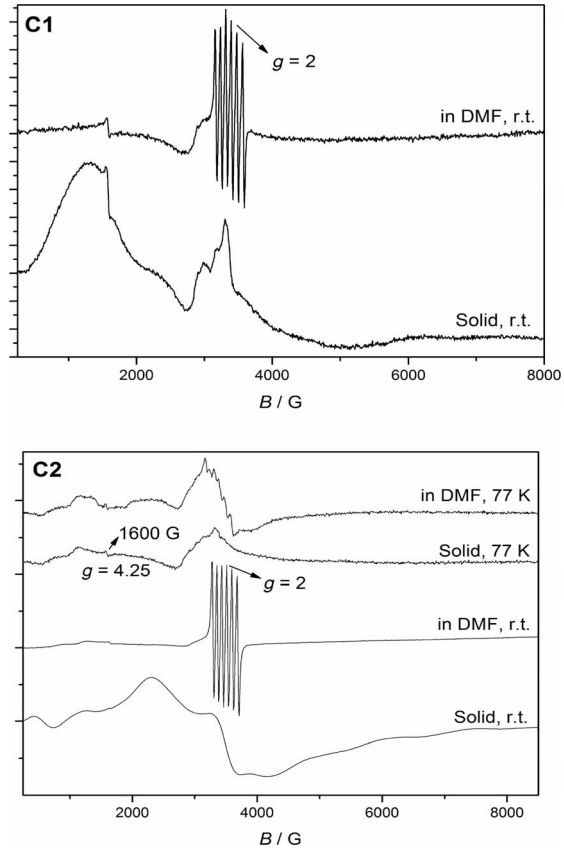

Figure 6. EPR of the complexes **C1** and **C2** (exp. conditions given in the graph).

EPR measurements of **C1**–**C4** were performed. The fluid solution spectra of **C1** and **C2** are dominated by the 6-lines pattern at $g = 2$, significant for the isotropic hyperfine splitting of one Mn^{II} nucleus ($I = 5/2$) spaced by the corresponding hyperfine coupling constant of ca. 80 G. The frozen solution spectra (77 K) as well as the signals obtained from the parent solid samples reveal additional, significantly intense signals in the $g = 4$ region. For **C2**, weak features at even lower field (750 G) indicate that even interactions by more than two Mn^{II} nuclei are likely to be present both in frozen solution and in the powder samples.[25] These EPR spectra which span over a substantial range of g factors are likely to be caused by overlapping contributions of different spin manifolds. Whereas the intense signal at $g \approx 2$ is due to $\Delta M_s = \pm 1$ ($S = 1/2$), $\Delta M_s = \pm 2$ transitions ($S = 1$) are visible around 1600 G and the signals at lower field are in line with even higher spin states. Thus, the fluid solution spectra (in DMF) of **C1** and **C2** suggest that under these conditions a dominant number of the complexes dissociates into (mononuclear) species. The communication between two or more Mn^{II} centers established for the frozen state and in the parent powder samples cannot be rigorously excluded for the fluid state, since under fluid solution conditions the interaction between Mn^{II} atoms is not detectable (Figure 6).

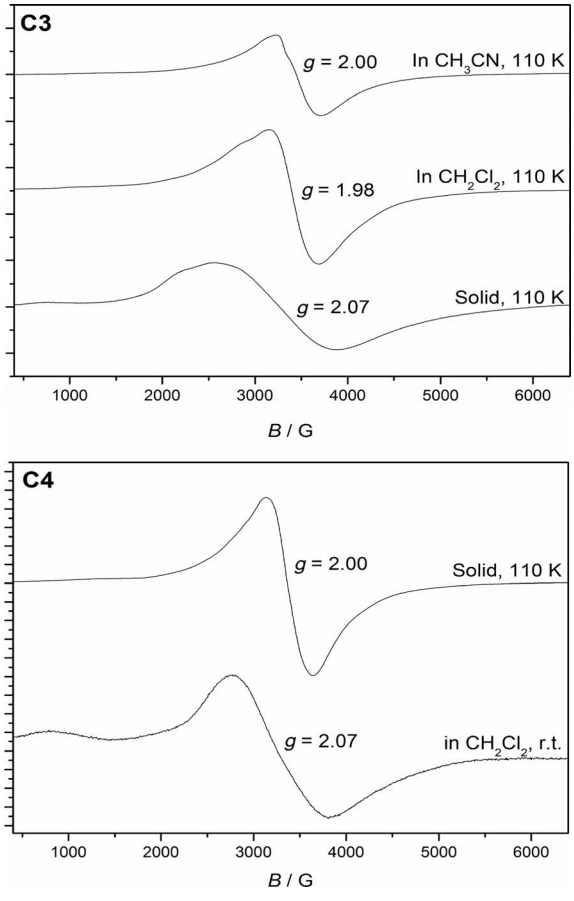

Figure 7. EPR of the complexes **C3** and **C4** (exp. conditions given in the graph).

The EPR spectra of **C3** and **C4** were measured in the solid state as well as in dichloromethane at 295 K and 110 K (**C3** also measurements in acetonitrile solution at 110 K). The similarity of the spectra at 295 K and 110 K suggests that similar spin manifolds are populated at both temperatures. All the spectra are broad, and hyperfine coupling to the Mn nuclei ($I = 5/2$) is not observed. This feature is typical for trinuclear Mn^{II} complexes and has been observed previously.[21a,26] Strong intermolecular dipolar interaction as well as overlap of signals from many different spin manifolds result in the loss of hyperfine information and broadening of the signals. The strong central signal can be attributed to an allowed $\Delta M = \pm 1$ transition. The signal at lower field which is weak in nature can be attributed to a forbidden $\Delta M \geq \pm 2$ transition. In contrast to **C1** and **C2**, which clearly decompose in solution to show the typical six-line pattern for a mononuclear Mn^{II} complex, the spectra of **C3** and **C4** indicate that their polynuclearity is maintained in solution. The signals of **C3** and **C4** are thus also broad and featureless in frozen solution. The intensity of the forbidden transition (low field) is much weaker in solution than the solid-state measurements as would be expected for measurements in solution (Figure 7).

Epoxidation Experiments

For the first screening of our (hybrid guanidine)manganese complexes we chose the epoxidation of the terminal olefin 1-octene as test reaction, because 1,2-epoxides are versatile starting materials in a multitude of syntheses.[27] 1-Octene is a well-established test substrate for first investigations of a new catalyst class and it has been studied by several groups.[2–4,7] It represents a standard model system and has a good analytical basis. In situ prepared mixtures of the ligand and equimolar amounts of the manganese source or the isolated complexes (1 mol-%) in CH_3CN were used as catalyst. Besides the standard manganese sources manganese chloride and manganese acetate, we tested manganese triflate because it has been successfully used by others.[3,6,7] As oxygen source we utilized a milder peracetic acid (PAA_R, 8–9%) prepared with a strongly acidic resin instead of H_2SO_4, like Stack et al. and other groups used before.[3,5]

Initially we investigated the combination of DMEGqu and $Mn(CH_3COO)_2{\cdot}4H_2O$ as catalyst. This system showed promising catalytic activity (Table 3). After 5 min at 0 °C the yield is already 40% whereas at room temperature the yield was determined to 52% with a conversion of 70%. This is consistent with a turn over number (TON: mol of 1-octene converted per mol of Mn) of 700 and a turn over frequency (TOF stands for TON per second) of 2.23 s^{-1}. After 30 min at room temperature the yield amounts to 65% and the conversion is 89%. The TON at this condition is 890 and the TOF value is 0.49 s^{-1}. The control experiment without catalyst gave never yields higher than 5% under the tested conditions (Figure 8). The use of the appropriate ratio of ligand to manganese source and the use of

Table 3. Catalytic epoxidation[a] of 1-octene by (guanidine)manganese complexes with PAA_R.

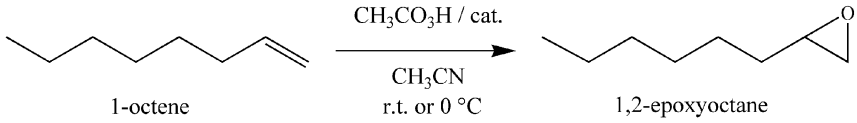

	0 °C								Room temperature							
	5 min				30 min				5 min				30 min			
	Yield [%]	Conv. [%]	TON	TOF [s^{-1}]	Yield [%]	Conv. [%]	TON	TOF [s^{-1}]	Yield [%]	Conv. [%]	TON	TOF [s^{-1}]	Yield [%]	Conv. [%]	TON	TOF [s^{-1}]
L1	40	57	570	1.90	54	75	750	0.42	52	70	700	2.33	65	89	890	0.49
L2	36	54	540	1.80	51	71	710	0.39	46	67	670	2.23	62	85	850	0.47

[a] Reaction conditions: 1 mL in situ prepared mixtures of the ligand and equimolar amounts of manganese acetate (5 mM), alkene (0.5 mmol), 2 equiv. CH_3CO_3H (dropwise addition). Yields and conversions were determined with GC analysis relative to tetradecane as internal standard on basis of an average of at least three runs.

the isolated complex **C1** leads to the same results like the in situ formed 1:1 catalyst. The use of the isolated complex **C2** containing TMGqu as ligand does not lead to a significant change of yield.

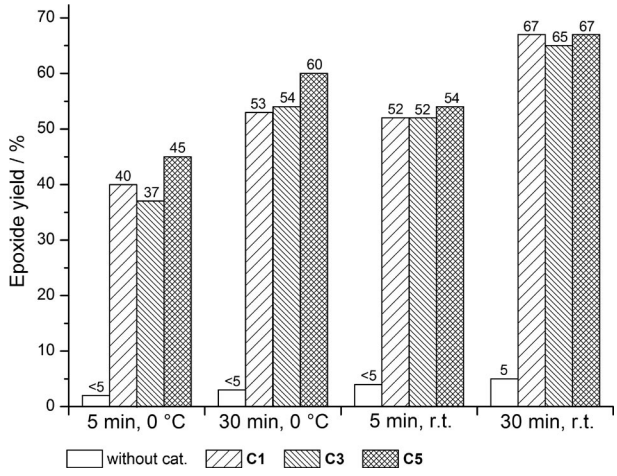

Figure 8. Influence of the manganese source on the epoxidation of 1-octene. Reaction conditions: To a solution of the complex (5 μmol based on Mn) in 1 mL of CH_3CN and 1-octene (0.5 mmol), 2 equiv. CH_3CO_3H were added dropwise.

The next step was to study the influence of the manganese source. Therefore the catalytic activity of **C3** and **C5** were determined. At room temperature no significant differences could be observed. Only at 0 °C **C5** showed increasing yields (Figure 8). The use of the in situ formed complexes leads to the same results. It is remarkable that the solids of the complexes **C1**–**C4** are very stable. The yellow and orange powders did not loose their catalytic activity even after months on air. Further investigations were focused on the temporal progress of the epoxidation with the DMEGqu/$Mn(CH_3COO)_2$ system at 0 °C (Figure 9). After 2 min already 34% yield of the epoxide were formed and after 60 min the reaction is nearly finished (68% yield).

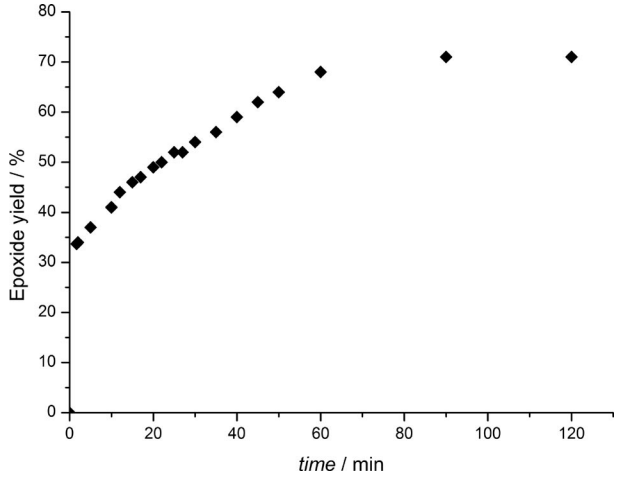

Figure 9. Yield of 1-epoxyoctane during the epoxidation with **C3** in CH_3CN at 0 °C with 2 equiv. of PAA_R.

In summary, the findings show that the manganese complexes reported here exhibit a good epoxidation activity. It has to be remarked that the activity is not affected by the anionic component or by the nuclearity of the used (guanidine)manganese complexes which definitely changes in case of **C1** and **C2** upon dissolution while **C3** and **C4** are polynuclear in solution. The structural situation in the epoxidation solution in the presence of peracetic acid (which is supposed to coordinate to the manganese)[1] is probably even more complicated. Due to the similarity in catalytic activity, we propose that the active species for all complexes presented here might be mononuclear (guanidine)manganese–peracetic acid adducts.

Comparing the presented epoxidation results with already reported results has to take into account that the experimental conditions strongly influence yield and conversion. For this reason, a direct comparison is only possible with the results reported by Stack et al. using peracetic acid made on resin.[3c] This group studied the epoxidation of 1-octene with several amines as stabilising ligands. The re-

ported yields of epoxyoctane after 5 min reaction time lie in the range of 11 to 96% and the conversion between 11 and 99%. Our results show with 52% yield and 79% conversion (**C3**) a good position in the upper middle range. Taking into account their robustness and simple preparation, the presented epoxidation results open up a new ligand class for epoxidation chemistry.

Conclusions

In this contribution we report on the synthesis and complete characterisation of the first (guanidine–quinoline) manganese complexes with the hybrid guanidine ligands DMEGqu and TMGqu. Depending on the manganese source we observed different coordination motifs. The structural analysis revealed that the chlorido complexes display a dinuclear $Mn_2(\mu\text{-}Cl)_2Cl_2$ motif whereas the acetato complexes exhibit a trinuclear multi-acetato-bridged structure. The dinuclear triflato complex has a unique $Mn_2(\mu\text{-}CF_3SO_3)_2(CF_3SO_3)_2$ bridging unit. These complexes enrich the small series of reported (guanidine)manganese complexes by new polynuclear examples. EPR measurements gave an insight in the behaviour upon dissolution in polar aprotic solvents. The chlorido complexes **C1** and **C2** dissociate into mononuclear species whereas the acetato complexes maintain a polynuclear structure. Remarkably, these complexes all show catalytic activity in the epoxidation of the terminal alkene 1-octene. Screening of the variation of manganese components and guanidine units within the catalysts has proven that the catalytic activity is for all tested systems comparably high. Comparison of in-situ-prepared and isolated compounds shows the same activity for both. The acetato and chlorido complexes are very stable at air and can be stored long time without losing their catalytic activity. This makes the systems easily applicable under industrial conditions.

Experimental Section

Materials and Methods: The preparation of the ligands and complexes were performed under nitrogen dried with P_4O_{10} granulate using Schlenk techniques or in a glove box. Solvents were purified according to literature procedures and kept under nitrogen. $MnCl_2{\cdot}4H_2O$, $Mn(CH_3COO)_2{\cdot}4H_2O$, 1-octene and tetradecane were used without further purification. $Mn(CF_3SO_3)_2{\cdot}H_2O$,[28] *N*-(1,3-dimethylimidazolin-2-ylidene)quinolin-8-amine (DMEGqu, **L1**),[14] 1,1,3,3-tetramethyl-2-(quinolin-8-yl)guanidine (TMGqu, **L2**)[14] and PAA_R[3c,29] were prepared according to literature procedures.

Instrumentation: IR spectra were recorded on a Nicolet P510 FT-IR using KBr pellets as matrix. EI mass spectra were performed with a Finnigan MAT95 spectrometer (70 eV). Elemental analyses were measured with an Elementar vario MICRO Cube analyzer and fluorine-containing compounds with an analyzer CHNS-932 from Leco. GC analysis was performed by using a Agilent 6890N gas chromatograph with FID detector. EPR spectra were taken on a Bruker ESP 300 Instrument (**C1**, **C2**) and a Bruker system EMX (**C3**, **C4**). The fluid solution samples (DMF dried with molecular sieves) were degassed by 3–4 freeze-thaw cycles on a vacuum line. For the EPR spectra at 77 K, the samples were placed into a Dewar finger filled with liquid nitrogen and placed inside the cavity of the EPR spectrometer.

Crystal Structure Analyses: Crystal data for compounds **C1**–**C5** are presented in Table 4. X-ray diffraction data were collected with a Bruker-AXS SMART APEX CCD, using Mo-K_α radiation (λ = 0.71073 Å) and a graphite monochromator. Data reduction and absorption correction was performed with SAINT and SADABS.[30] The structures were solved by direct and conventional Fourier

Table 4. Crystallographic details for compound **C1**–**C5**.

	C1	**C2**	**C3**	**C4**	**C5**
Empirical formula	$C_{28}H_{32}Cl_4Mn_2N_8$	$C_{28}H_{36}Cl_4Mn_2N_8$	$C_{40}H_{50}Mn_3N_8O_{12}$	$C_{40}H_{54}Mn_3N_8O_{12}$	$C_{32}H_{36}F_{12}Mn_2N_8O_{14}S_4$
Molecular mass	732.30	736.32	999.70	1003.73	1222.81
Crystal size [mm]	0.40 × 0.37 × 0.32	0.43 × 0.40 × 0.29	0.43 × 0.40 × 0.38	0.37 × 0.32 × 0.25	0.48 × 0.47 × 0.39
Crystal system	monoclinic	monoclinic	monoclinic	triclinic	triclinic
Space group	$P2_1/c$	$P2_1/n$	$P2_1/c$	$P\bar{1}$	$P\bar{1}$
a [Å]	12.2144(19)	9.1542(11)	10.5453(15)	9.8166(18)	10.4733(16)
b [Å]	9.7785(15)	10.5521(12)	11.3913(16)	10.6824(19)	11.3259(17)
c [Å]	13.485(2)	17.536(2)	18.528(2)	11.280(2)	11.3655(18)
α [°]	90	90	90	71.170(3)	106.756(3)
β [°]	91.086(3)	103.987(3)	101.503(3)	82.950(4)	103.870(3)
γ [°]	90	90	90	85.028(4)	106.418(3)
V [Å^3]	1610.4(4)	1643.7(3)	2180.9(5)	1109.7(3)	1160.1(3)
Z	2	2	2	1	1
$D_{calcd.}$ [g/cm^3]	1.510	1.488	1.522	1.502	1.750
μ(Mo-K_α) [mm^{-1}]	1.149	1.126	0.926	0.910	0.844
Temperature [K]	243(2)	120(2)	120(2)	120(2)	120(2)
Data coll. range Θ [°]	1.67–27.88	2.27–27.88	1.97–27.88	1.92–26.37	2.00–26.37
h,*k*,*l*	–15/16,±12,±17	±12,±13,±23	±13,±14,±24	–12/11,±13,±14	±13,–14/9,–11/14
Reflections measured	13820	14215	18718	7532	6700
Unique data	3829	3913	5199	4463	4539
Parameters	192	194	291	293	335
*R*1 [$I \geq 2\sigma(I)$]	0.0315	0.0304	0.0328	0.0465	0.0295
*wR*2 (all data)	0.0890	0.0756	0.0860	0.1164	0.0829
min./max. Δ*F* [e/Å^3]	–0.323/0.534	–0.277/0.477	–0.232/0.338	–0.633/0.543	–0.378/0.355

methods and all non-hydrogen atoms refined anisotropically with full-matrix least-squares based on F^2 (SHELXTL[30]). H-atom positions were clearly derived from difference Fourier maps, then included in the refinement at ideal positions based on the riding model. Due to phase transition at about 235 K data for **C1** were collected at 243(2) K.

CCDC-742745 (for **C1**), -742746 (for **C2**), -742747 (for **C3**), -742748 (for **C4**) and -742749 (for **C5**) contain the supplementary crystallographic data for this paper. These data can be obtained free of charge from The Cambridge Crystallographic Data Centre via www.ccdc.cam.ac.uk/data_request/cif.

Preparation of Compounds

$[Mn_2(DMEGqu)_2(\mu\text{-}Cl)_2Cl_2]$ (C1): To a solution of DMEGqu (0.120 g, 0.5 mmol) in 3 mL of absol. CH_3CN, $MnCl_2{\cdot}4H_2O$ (0.099 g, 0.5 mmol) with 2 mL of CH_3CN was added whilst stirring. A yellow solid was observed; yield 82% (0.15 g). Orange red crystals suitable for X-ray diffraction could be obtained by crystallisation from hot CH_3CN. IR (KBr): $\tilde{\nu}$ = 3055 *vw* [$\nu(CH)_{arom.}$], 3003 *vw* [$\nu(CH)_{arom.}$], 2947 *w* [$\nu(CH)_{aliph.}$], 2885 *w* [$\nu(CH)_{aliph.}$], 2796 *vw* [$\nu(CH)_{aliph.}$], 2360 *vw*, 1601 *m* [ν(C=N)], 1562 vs. [ν(C=N)], 1540 *s* [ν(C=N)], 1502 vs, 1479 *m*, 1466 *s*, 1416 *m*, 1389 *s*, 1323 *w*, 1288 *m*, 1236 *m*, 1207 *vw*, 1103 *w*, 1026 *m*, 978 *w*, 906 *vw*, 831 *w*, 816 *m*, 804 *w*, 785 *m*, 758 *w*, 688 *w*, 640 *w*, 579 *w*, 532 *vw* cm^{-1}. EI-MS [*m*/*z*, (%)]: 241 (24) [$DMEGqu^+$ + H], 240 (100) [$DMEGqu^+$], 239 (76), 225 (5) [$DMEGqu^+$-CH_3], 184 (10) [$MnNC_9H_6^+$ + H], 183 (14) [$MnNC_9H_6^+$], 182 (7),169 (12), 157 (8), 156 (7), 155 (41), 154 (6), 144 (7), 143 (11) [$N_2C_9H_6^+$ + H], 142 (13) [$N_2C_9H_6^+$], 129 (22) [$NC_9H_6^+$ + H], 128 (12) [$NC_9H_6^+$], 127 (5), 120 (6), 101 (6), 98 (50) [$CN_2(CH_3)_2(CH_2)_2^+$], 69 (5), 42 (8). $C_{28}H_{32}Cl_4Mn_2N_8$ (732.30): calcd. C 45.92, H 4.41, N 15.30; found C 46.03, H 4.42, N 15.26.

$[Mn_2(TMGqu)_2(\mu\text{-}Cl)_2Cl_2]$ (C2): To a solution of TMGqu (0.121 g, 0.5 mmol) in 3 mL of absol. CH_3CN $MnCl_2{\cdot}4H_2O$ (0.099 g, 0.5 mmol) with 2 mL of CH_3CN was added whilst stirring. An orange solid was observed; yield 87% (0.16 g). Red crystals suitable for X-ray diffraction was obtained by crystallisation from hot CH_3CN. IR (KBr): $\tilde{\nu}$ = 3045 *vw* [$\nu(CH)_{arom.}$], 3006 *vw* [$\nu(CH)_{arom.}$], 2949 *w* [$\nu(CH)_{aliph.}$], 2927 *w* [$\nu(CH)_{aliph.}$], 2892 *vw* [$\nu(CH)_{aliph.}$], 2866 *vw* [$\nu(CH)_{aliph.}$], 2796 *vw* [$\nu(CH)_{aliph.}$], 1568 *s* [ν(C=N)], 1518 vs. [ν(C=N)], 1500 vs. [ν(C=N)], 1466 vs, 1410 *m*, 1398 vs, 1384 *m*, 1378 *m*, 1324 *s*, 1269 *w*, 1236 *m*, 1159 *m*, 1097 *w*, 1077 *w*, 1020 *m*, 920 *vw*, 897 *vw*, 837 *m*, 827 *m*, 806 *w*, 793 *m*, 769 *m*, 752 *w*, 700 *m*, 654 *vw*, 627 *w*, 588 *w*, 540 *w* cm^{-1}. EI-MS [*m*/*z* (%)]: 367 (5) [$(M/2)^+$: $C_{14}H_{18}N_4Cl_2Mn$], 332 (6) [$(M/2)^+ - Cl_2$], 243 (15) [$TMGqu^+$ + H], 242 (100) [$TMGqu^+$], 227 (6) [$TMGqu^+$-CH_3], 199 (15), 198 (79), 184 (31), 183 (15), 182 (16), 172 (7), 171 (41), 169 (8), 157 (33), 156 (24), 155 (80), 143 (15) [$N_2C_9H_6^+$ + H], 142 (15) [$N_2C_9H_6^+$], 129 (23) [$NC_9H_6^+$ + H], 128 (13) [$NC_9H_6^+$], 116 (5), 100 (29) [$C(N(CH_3)_2)_2^+$], 85 (5), 44 (8), 42 (6). $C_{28}H_{36}Cl_4Mn_2N_8$ (736.33): calcd. C 45.67, H 4.93, N 15.22; found C 45.68, H 4.88, N 15.19.

$[Mn_3(DMEGqu)_2(\mu\text{-}CH_3COO)_6]$ (C3): To a solution of DMEGqu (0.120 g, 0.5 mmol) in 3 mL of absol. CH_3CN $Mn(CH_3COO)_2{\cdot}4H_2O$ (0.123 g, 0.5 mmol) with 2 mL of CH_3CN was added whilst stirring. A yellow solid was observed; yield 72% (0.12 g). Amber crystals suitable for X-ray diffraction was obtained by gas phase diffusion of diethyl ether. IR (KBr): $\tilde{\nu}$ = 3055 *vw* [$\nu(CH)_{arom.}$], 2970 *vw* [$\nu(CH)_{aliph.}$], 2924 *w* [$\nu(CH)_{aliph.}$], 2873 *vw* [$\nu(CH)_{aliph.}$], 1599 vs. [ν(C=N)], 1572 vs. [ν(C=N)], 1500 *m*, 1483 *m*, 1464 *m*, 1417 *s*, 1388 *s*, 1321 *m*, 1286 *w*, 1236 *w*, 1101 *w*, 1028 *m*, 976 *vw*, 928 *vw*, 812 *w*, 781 *w*, 750 *vw*, 689 *w*, 650 *w*, 613 *w*, 534 *vw* cm^{-1}. EI-MS [*m*/*z* (%)]: 241 (42) [$DMEGqu^+$ + H], 240 (100) [$DMEGqu^+$], 239 (86), 225 (11) [$DMEGqu^+$-CH_3], 211 (7), 197 (5), 196 (7), 184 (9) [$MnNC_9H_6^+$ + H], 183 (16) [$MnNC_9H_6^+$], 182 (7), 169 (12), 168 (5), 167 (9), 157 (9), 156 (7), 155 (37), 154 (7), 144 (6), 143 (11) [$N_2C_9H_6^+$ + H], 142 (14) [$N_2C_9H_6^+$], 129 (21) [$NC_9H_6^+$ + H], 128 (12) [$NC_9H_6^+$], 127 (5), 120 (7), 101 (6), 98 (49) [$CN_2(CH_3)_2(CH_2)_2^+$]. $C_{40}H_{50}Mn_3N_8O_{12}$ (999.69): calcd. C 48.05, H 5.00, N 11.21; found C 47.65, H 4.97, N 11.26.

$[Mn_3(TMGqu)_2(\mu\text{-}CH_3COO)_6]$ (C4): To a solution of TMGqu (0.121 g, 0.5 mmol) in 3 mL of absol. CH_3CN $Mn(CH_3COO)_2{\cdot}4H_2O$ (0.123 g, 0.5 mmol) with 2 mL of CH_3CN was added whilst stirring. A yellow solid precipitated; yield 60% (0.10 g). Yellow crystals suitable for X-ray diffraction could be obtained by gas phase diffusion of diethyl ether. IR (KBr): $\tilde{\nu}$ = 3049 *vw* [$\nu(CH)_{arom.}$], 3003 *vw* [$\nu(CH)_{arom.}$], 2929 *w* [$\nu(CH)_{aliph.}$], 2897 *vw* [$\nu(CH)_{aliph.}$], 2866 *vw* [$\nu(CH)_{aliph.}$], 2794 *vw* [$\nu(CH)_{aliph.}$], 1597 vs. [ν(C=N)], 1570 *s* [ν(C=N)], 1543 *m*, 1520 *s*, 1498 *m*, 1437 *m*, 1415 vs, 1385 *s*, 1336 *m*, 1275 *vw*, 1234 *w*, 1159 *m*, 1099 *w*, 1061 *w*, 1018 *m*, 939 *vw*, 831 *w*, 810 *w*, 786 *m*, 742 *w*, 698 *w*, 675 *w*, 654 *w*, 617 *vw*, 542 *vw* cm^{-1}. EI-MS [*m*/*z* (%)]: 243 (18) [$TMGqu^+$ + H], 242 (100) [$TMGqu^+$], 227 (7) [$TMGqu^+$-CH_3], 199 (16), 198 (66), 184 (31), 183 (17), 182 (15), 172 (7), 171 (36), 169 (9), 157 (29), 156 (22), 155 (64), 143 (13) [$N_2C_9H_6^+$ + H], 142 (13) [$N_2C_9H_6^+$], 129 (19) [$NC_9H_6^+$ + H], 128 (11) [$NC_9H_6^+$], 101 (5), 100 (16) [$C(N(CH_3)_2)_2^+$], 58 (11), 44 (19), 43 (51), 42 (7). $C_{40}H_{54}Mn_3N_8O_{12}$ (1003.72): calcd. C 47.86, H 5.42, N 11.16; found C 47.38, H 5.31, N 11.19.

$[Mn_2(DMEGqu)_2(\mu\text{-}CF_3SO_3)_2(CF_3SO_3)_2(H_2O)_2]$ (C5): To a solution of DMEGqu (0.120 g, 0.5 mmol) in 2 mL of absol. CH_3CN, $Mn(CF_3SO_3)_2{\cdot}H_2O$ (0.149 g, 0.5 mmol) in 2 mL of CH_3CN was added whilst stirring with 3 mL of CH_3CN. Yellow crystals suitable for X-ray diffraction could be obtained by crystallisation from a saturated CH_3CN solution. IR (KBr): $\tilde{\nu}$ = 2935 *w*, [ν(C–H)], 2889 *m* [ν(C–H)], 1599 *s* [ν(C=N)], 1572 [ν(C=N)], *s*, 1545 *s*, 1504 *s*, 1481 *m*, 1462 *m*, 1417 *m*, 1394 *s*, 1323 *m*, 1296 vs, 1261 vs, 1232 vs, 1188 *s*, 1176 *s*, 1103 *m*, 1029 vs, 978 *w*, 906 *w*, 833 *m*, 818 *m*, 804 *m*, 785 *m*, 762 *m*, 694 *w*, 642 s, 629 *s*, 580 *m*, 519 *m* cm^{-1}. EI-MS [*m*/*z* (%)]: 445 (7), 444 (35) [$DMEGquMnCF_3SO_3^+$], 314 (12), 294 (7), 241 (29) [$DMEGqu + H^+$], 240 (100) [$DMEGqu^+$], 239 (60), 225 (7) [$DMEGqu^+$-CH_3], 197 (5), 196 (5), 184 (6) [$MnNC_9H_6^+$ + H], 183 (10) [$MnNC_9H_6^+$], 182 (5), 169 (7), 167 (9), 157 (8), 156 (5), 155 (21), 144 (36), 143 (9) [$N_2C_9H_6^+$ + H], 142 (9) [$N_2C_9H_6^+$], 129 (13) [$NC_9H_6^+$ + H], 128 (5) [$NC_9H_6^+$], 120 (8), 117 (11), 116 (5), 98 (57) [$CN_2(CH_3)_2(CH_2)_2^+$], 69 (5), 59 (5). $C_{32}H_{36}F_{12}Mn_2N_8O_{14}S_4$ (1222.79): calcd. C 31.43, H 2.97, N 9.16; found C 31.0, H 3.0, N 9.0.

General Procedure for the Epoxidation of 1-Octene: 1 mL of the in-situ-formed complex (0.5 mM in CH_3CN) or 5 μmol of the isolated complex (based on Mn) in 1 mL of CH_3CN, 80 μL 1-octene (0.5 mol) and 50 μL tetradecane (internal standard) were mixed in a Schlenk tube at reaction temperature. Peracetic acid (8–9%, 1 mmol) was added dropwise over 90 s. After stirring for 5 or 30 min, the mixture was diluted with Et_2O, filtered through a basic alumina plug and prepared for GC analysis. The epoxide product was identified by comparison of the GC retention time of an authentic sample. GC conditions: 60 °C (3 min), 15 °C/min to 180 °C (2 min) on DB-5 column; 1-octene: R_t = 2.876 min, 1,2-epoxyoctane: R_t = 6.119 min, tetradecane: R_t = 10.368 min.

Acknowledgments

Financial support by the Fonds der Chemischen Industrie (Liebig fellowship to S. H.-P.) is gratefully acknowledged. Furthermore, we thank Prof. T. Daniel P. Stack for fruitful discussions.

[1] For examples, see: a) K. A. Jørgensen, *Chem. Rev.* **1989**, *89*, 431–458; b) T. Katsuki, *Coord. Chem. Rev.* **1995**, *140*, 189–214; c) J. Brinksma, R. Hage, J. Kerschner, B. L. Feringa, *Chem. Commun.* **2000**, 537–538; d) B. S. Lane, K. Burgess, *Chem. Rev.* **2003**, *103*, 2457–2473; e) J.-E. Bäckvall (Ed.), *Modern Oxidation Methods*, Wiley-VCH, Weinheim, Germany, **2004**; f) M. Beller, C. Bolm (Eds.), *Transition Metals for Organic Synthesis*, Wiley-VCH, Weinheim, Germany, **2004**; g) E. M. McGarrigle, D. G. Gilheany, *Chem. Rev.* **2005**, *105*, 1563–1602.

[2] K.-P. Ho, W.-L. Wong, K.-M. Lam, C. P. Lai, T. H. Chan, K.-Y. Wong, *Chem. Eur. J.* **2008**, *14*, 7988–7996.

[3] a) A. Murphy, G. Dubois, T. D. P. Stack, *J. Am. Chem. Soc.* **2003**, *125*, 5250–5251; b) A. Murphy, A. Pace, T. D. P. Stack, *Org. Lett.* **2004**, *6*, 3119–3122; c) A. Murphy, T. D. P. Stack, *J. Mol. Catal. A* **2006**, *251*, 78–88; d) T. J. Terry, T. D. P. Stack, *J. Am. Chem. Soc.* **2008**, *130*, 4945–4953; e) G. Dubois, A. Murphy, T. D. P. Stack, *Org. Lett.* **2003**, *5*, 2469–2472; f) T. J. Terry, G. Dubois, A. Murphy, T. D. P. Stack, *Angew. Chem. Int. Ed.* **2007**, *46*, 945–947.

[4] B. Kang, M. Kim, J. Lee, Y. Do, S. Chang, *J. Org. Chem.* **2006**, *71*, 6721–6727.

[5] G. Ilyashenko, D. Sale, M. Motevalli, M. Watkinson, *J. Mol. Catal. A* **2008**, *296*, 1–8.

[6] J. Rich, M. Rodríguez, I. Romero, L. Vaquer, X. Sala, A. Llobet, M. Corbella, M.-N. Collomb, X. Fontrodona, *Dalton Trans.* **2009**, 8117–8126.

[7] a) L. Gomez, I. Garcia-Bosch, A. Company, X. Sala, X. Fontrodona, X. Ribas, M. Costas, *Dalton Trans.* **2007**, 5539–5545; b) I. Garcia-Bosch, A. Company, X. Fontrodona, X. Ribas, M. Costas, *Org. Lett.* **2008**, *10*, 2095–2098.

[8] a) B. Meunier (Ed.), *Metal-Oxo and Peroxo Species*, Springer-Verlag, Berlin, Heidelberg, Germany, **2000**; b) W. Ando (Ed.), *Organic Peroxides*, Wiley-VCH, Chichester, U.K., **1992**.

[9] a) S. Herres-Pawlis, U. Flörke, G. Henkel, *Eur. J. Inorg. Chem.* **2005**, 3815–3824; b) S. Herres-Pawlis, P. Verma, R. Haase, P. Kang, C. T. Lyons, E. C. Wasinger, U. Flörke, G. Henkel, T. D. P. Stack, *J. Am. Chem. Soc.* **2009**, *131*, 1154–1169; c) M. Schatz, V. Raab, S. P. Foxon, G. Brehm, S. Schneider, M. Reiher, M. C. Holthausen, J. Sundermeyer, S. Schindler, *Angew. Chem. Int. Ed.* **2004**, *43*, 4360–4363; d) C. Würtele, E. Gaoutchenova, K. Harms, M. C. Holthausen, J. Sundermeyer, S. Schindler, *Angew. Chem. Int. Ed.* **2006**, *45*, 3867–3869; e) D. Maiti, D.-H. Lee, K. Gaoutchenova, C. Würtele, M. C. Holthausen, A. A. Narducci Sarjeant, J. Sundermeyer, S. Schindler, K. D. Karlin, *Angew. Chem. Int. Ed.* **2008**, *47*, 82–85; f) J. England, M. Martinho, E. R. Farquhar, J. R. Frisch, E. L. Bominaar, E. Münck, L. Que Jr., *Angew. Chem. Int. Ed.* **2009**, *48*, 3622–3626; g) A. Peters, U. Wild, O. Hübner, E. Kaifer, H.-J. Himmel, *Chem. Eur. J.* **2008**, *14*, 7813–7821; h) D. Petrovic, L. M. R. Hill, P. G. Jones, W. B. Tolman, M. Tamm, *Dalton Trans.* **2008**, 887–894.

[10] A. Neuba, O. Seewald, U. Flörke, G. Henkel, *Acta Crystallogr., Sect. E* **2007**, *63*, m2099–m2100.

[11] a) A. Neuba, S. Herres-Pawlis, U. Flörke, G. Henkel, *Z. Allg. Anorg. Chem.* **2008**, *634*, 771–777; b) A. Neuba, R. Haase, M. Bernard, U. Flörke, S. Herres-Pawlis, *Z. Anorg. Allg. Chem.* **2008**, *634*, 2511–2517; c) A. Neuba, S. Herres-Pawlis, O. Seewald, J. Börner, A. J. Heuwing, U. Flörke, G. Henkel, *Z. Anorg. Allg. Chem.* **2010**, DOI: 10.1002/zaac.201000133.

[12] a) H. Wittmann, Ph. D. Thesis, Universität Marburg, **1999**; b) H. Wittmann, A. Schorm, J. Sundermeyer, *Z. Anorg. Allg. Chem.* **2000**, *626*, 1583–1590; c) H. Wittmann, V. Raab, A. Schorm, J. Plackmeyer, J. Sundermeyer, *Eur. J. Inorg. Chem.* **2001**, 1937–1948; d) V. Raab, Ph. D. Thesis, Universität Marburg, Germany, **2001**.

[13] S. Herres-Pawlis, A. Neuba, O. Seewald, T. Seshadri, H. Egold, U. Flörke, G. Henkel, *Eur. J. Org. Chem.* **2005**, 4879.

[14] A. Hoffmann, J. Börner, U. Flörke, S. Herres-Pawlis, *Inorg. Chim. Acta* **2009**, *362*, 1185–1193.

[15] A. W. Addison, T. N. Rao, J. Reedijk, J. van Rijn, G. C. Verschoor, *J. Chem. Soc., Dalton Trans.* **1984**, 1349–1356.

[16] For examples, see: a) A. Garoufis, S. Kasselouri, S. Boyatzis, C. P. Raptopoulou, *Polyhedron* **1999**, *18*, 1615–1620; b) I. Romero, M.-N. Collomb, A. Deronzier, A. Llobet, E. Perret, J. Pécaut, L. Le Pape, J.-M. Latour, *Eur. J. Inorg. Chem.* **2001**, 69–72; c) D. Armentano, G. de Munno, F. Guerra, J. Faus, F. Lloret, M. Julve, *Dalton Trans.* **2003**, 4626–4634; d) G. A. Van Albada, A. Mohamadou, W. L. Driessen, R. De Gelder, S. Tanase, J. Reedijk, *Polyhedron* **2004**, *23*, 2387–2391; e) J.-Z. Wu, E. Bouwman, A. M. Mills, A. L. Spek, J. Reedijk, *Inorg. Chim. Acta* **2004**, *357*, 2694–2702; f) C. J. Davies, J. Fawcett, R. Shutt, G. A. Solan, *Dalton Trans.* **2005**, 2630–2640; g) C.-M. Qi, X.-X. Sun, S. Gao, S.-L. Ma, D.-Q. Yuan, C.-H. Fan, H.-B. Huang, W.-X. Zhu, *Eur. J. Inorg. Chem.* **2007**, 3663–3668.

[17] a) I. Romero, M. Rodríguez, A. Llobet, M. Corbella, G. Fernández, M.-N. Collomb, *Inorg. Chim. Acta* **2005**, *358*, 4459–4465; b) J.-Z. Wu, S. Tanase, E. Bouwman, J. Reedijk, A. M. Mills, A. L. Spek, *Inorg. Chim. Acta* **2003**, *351*, 278–282.

[18] X.-M. Lu, P.-Z. Li, X.-T. Wang, S. Gao, X.-J. Wang, L. Zhou, C.-S. Liu, X.-N. Sui, J.-H. Feng, Y.-H. Deng, Q.-H. Jin, J. Liu, N. Liu, J.-P. Lian, *Polyhedron* **2008**, *27*, 3669–3673.

[19] a) E. Sinn, *J. Chem. Soc., Dalton Trans.* **1976**, *2*, 162–165; b) D. I. Arnold, F. A. Cotton, D. J. Maloney, J. H. Matonic, *Polyhedron* **1997**, *16*, 133–141; c) X.-Y. Hou, J.-J. Wang, X. Wang, D.-S. Li, J.-W. Wang, *Z. Kristallogr. NCS* **2007**, *222*, 57–58.

[20] a) R. L. Rardin, W. B. Tolman, S. J. Lippard, *New J. Chem.* **1991**, *15*, 417–430; b) R. L. Rardin, A. Bino, P. Poganiuch, W. B. Tolman, S. Liu, S. J. Lippard, *Angew. Chem. Int. Ed. Engl.* **1990**, *29*, 812–814.

[21] a) D. P. Kessissoglou, *Coord. Chem. Rev.* **1999**, *185–186*, 837–858; b) M. Kloskowski, D. Pursche, R.-D. Hoffmann, R. Pöttgen, M. Läge, A. Hammerschmidt, T. Glaser, B. Krebs, *Z. Anorg. Allg. Chem.* **2007**, *633*, 106–111; c) R. L. Rardin, P. Poganiuch, A. Bino, D. P. Goldberg, W. B. Tolman, S. Liu, S. J. Lippard, *J. Am. Chem. Soc.* **1992**, *114*, 5240–5249; d) S. Ménage, S. E. Vitolis, P. Bergerat, E. Codjovi, O. Kahn, J.-J. Girerd, M. Guillot, X. Solans, T. Calvet, *Inorg. Chem.* **1991**, *30*, 2666–2671.

[22] V. Tangoulis, D. A. Malamatari, K. Soulti, V. Stergiou, C. P. Raptopoulou, A. Terzis, T. A. Kabanos, D. P. Kessissoglou, *Inorg. Chem.* **1996**, *35*, 4974–4983.

[23] E. F. Bertaut, T. Q. Duc, P. Burlet, M. Thomas, J. M. Moreau, *Acta Crystallogr., Sect. B* **1974**, *30*, 2234–2236.

[24] V. Raab, K. Harms, J. Sundermeyer, B. Kovacevic, Z. B. Maksic, *J. Org. Chem.* **2003**, *68*, 8790–8797.

[25] a) M. Brustolon, E. Giamello (Eds.), *Electron Paramagnetic Resonance: A Practitioners Toolkit*, Wiley & Sons, Chichester, **2009**; b) A. P. Golombek, M. P. Hendrich, *J. Magn. Reson.* **2003**, *165*, 33–48.

[26] L. David, C. Craciun, V. Chis, R. Tetean, *Solid State Commun.* **2002**, *121*, 675–678.

[27] S. E. Schaus, B. D. Brandes, J. F. Larrow, M. Tokunaga, K. B. Hansen, A. E. Gould, M. E. Furrow, E. N. Jacobsen, *J. Am. Chem. Soc.* **2002**, *124*, 1307–1315.

[28] Y. Inada, Y. Nakano, M. Inamo, M. Nomura, S. Funahashi, *Inorg. Chem.* **2000**, *39*, 4793–4801.

[29] A. T. Hawkinson, W. R. Schmitz, US 2,910,504, E. I. du Pont de Nemours & Co., **1959**.

[30] SMART (v. 5.62), SAINT (v. 6.02), SHELXTL (v. 6.10) and SADABS (v. 2.03), Bruker AXS Inc., Madison, Wisconsin, USA, **2002**.

Received: August 3, 2010
Published Online: December 2, 2010

